

Properties of atomic intercalated carbon K_4 crystals

Masahiro Itoh,^{1,2} Seiichi Takami,¹ Yoshiyuki Kawazoe,³ and Tadafumi Adachi^{1,2}

¹Institute of Multidisciplinary Research for Advanced Materials,
Tohoku University, Aoba-ku, Sendai 980-8577, Japan

²Advanced Institute for Materials Research, WPI,
Tohoku University, Aoba-ku, Sendai 980-8577, Japan

³Institute for Materials Research, Tohoku University, Aoba-ku, Sendai 980-8577, Japan

(Dated: February 22, 2024)

The stability of atomic intercalated carbon K_4 crystals, XC_2 ($X = H, Li, Be, B, C, N, O, F, Na, Mg, Al, Si, P, S, Cl, K, Ca, Ga, Ge, As, Se, Br, Rb$ or Sr) is evaluated by geometry optimization and frozen phonon analysis based on first principles calculations. Although CK_4 is unstable, NaC_2 and MgC_2 are found to be stable. It is shown that NaC_2 and MgC_2 are metallic and semiconducting, respectively.

PACS numbers:

I. INTRODUCTION

Recently, mathematical analysis elucidated that 120 bonding forms a 3-D 10-member ring periodic structure (K_4 structure) and can be regarded as the twin of the diamond structure¹. From the view point of carbon chemistry, 120 bonding is of the sp^2 bond type, which forms a 2-D structure with a 6-member ring, and the K_4 carbon structure has not been experimentally discovered. Because of the wide applications of carbon materials (graphite, amorphous, diamond, CNT and fullerene²), if such a new member exists in nature or can be synthesized, then this new material should have a very significant impact.

The stability and properties of this carbon K_4 structure have been studied using first principles calculations^{3,4}. It is interesting to note that carbon K_4 is metallic^{3,4}, although the phonon calculation results indicate the structure is unstable⁵. Compared with the graphite structure of sp^2 bonding, the binding energy per bond is slightly lower. This is possibly one of the reasons for the instability of the carbon K_4 crystals against the thermal vibration.

It is well understood that atomic intercalation to the carbonaceous materials changes the structural stability and sometimes provides totally different properties. We propose that atomic intercalation will affect the electronic distribution in the K_4 crystals and possibly stabilize the structure. Over 40 years ago, disilicides such as $SrSi_2$ were found to have K_4 type frame of Sf . This result encouraged us to investigate in purity intercalated carbon K_4 systems although such crystal structures are not found in the carbide system⁷.

This study examines the structural stability and several properties of the atomic intercalated carbon K_4 crystals, XC_2 ($X = H, Li, Be, B, C, N, O, F, Na, Mg, Al, Si, P, S, Cl, K, Ca, Ga, Ge, As, Se, Br, Rb$ or Sr) by first principles calculations.

II. COMPUTATIONAL METHODS

First principles calculations based on density functional theory^{8,9} are performed for the K_4 type crystals XC_2 , C , Si and $SrSi_2$ using the Vienna Ab-initio Simulation Package (VASP)¹⁰.

Local density approximation (LDA)^{11,12} is used for the exchange-correlation energy functional. In the present calculations, all these crystals are considered as spin-unpolarized systems.

To reduce the computational costs, the projector-augmented wave method¹³ is used to approximate electrons in each atom in the crystal. For $H, Li, Be, B, C, N, O, F, Na, Mg, Al, Si, P, S, Cl, K, Ca, Ga, Ge, As, Se, Br, Rb$ and Sr , valence electrons of $1s^1, 2s^1, 2s^2, 2s^2 2p^1, 2s^2 2p^2, 2s^2 2p^3, 2s^2 2p^4, 2s^2 2p^5, 3s^1, 3s^2, 3s^2 3p^1, 3s^2 3p^2, 3s^2 3p^3, 3s^2 3p^4, 3s^2 3p^5, 3s^2 3p^6 4s^1, 3s^2 3p^6 4s^2, 4s^2 4p^1, 4s^2 4p^2, 4s^2 4p^3, 4s^2 4p^4, 4s^2 4p^5, 4s^2 4p^6 5s^1$ and $4s^2 4p^6 5s^2$ are considered, respectively.

To evaluate the stability of the XC_2 K_4 crystal structure, the following procedure is adopted.

(1) The original conventional unit cell for the carbon K_4 crystal is shown in Figure 1(a). Four X atoms ($X = H, Li, Be, B, C, N, O, F, Na, Mg, Al, Si, P, S, Cl, K, Ca, Ga, Ge, As, Se, Br, Rb$, or Sr) are allocated to reduced coordinates $(\frac{1}{8}, \frac{1}{8}, \frac{1}{8}), (\frac{7}{8}, \frac{5}{8}, \frac{3}{8}), (\frac{2}{8}, \frac{7}{8}, \frac{5}{8}), (\frac{5}{8}, \frac{3}{8}, \frac{7}{8})$ in the original unit cell. The primitive unit cell of XC_2 with $P4_32$ (O^6) symmetry is shown in Fig. 1(b). The symmetric plane of the atomic intercalated system is shown in Fig. 1(c). As shown in Fig. 1(d), three adjacent atoms (red) are aligned on a straight line with the same distance ($C-X$, and $X-C$).

(2) Binding energy versus volume curve is evaluated and fitted using Murnaghan's equation of state¹⁴. For these calculations, Brillouin zone integration is performed for $8 \times 8 \times 8$ k-point meshes generated by the Monkhorst-Pack scheme. The residual minimization/direct inversion in the iterative subspace method is used to accelerate the convergence of self-consistent total energy calculations. The convergence criterion is set to

be within 1×10^{-8} eV/formula unit cell. The cut-off energy for the plane-wave expansion of valence electrons for the primitive unit cell is determined, so that the number of plane waves is constant over a full range of the lattice constant. Around the minimum of binding energy versus volume curve, the cut-off energies were set to be 500 and 400 eV for C and XC_2 , and Si and XS_2 crystals, respectively.

(3) The unit cells obtained from step (2) are optimized with freedom of the atomic configuration under the symmetry constraint.

(4) The unit cells obtained from step (3) are optimized without any constraint on the crystal structure. The convergence criterion is set to be within 1×10^{-7} eV/A unit cell.

(5) The frozen phonon calculations were performed using the FROPHO code¹⁵ which is based on Parlinski-Li-Kawazoe method¹⁶. To obtain the force constants for the phonon calculations, the atomic displacements are set to be 0.01 Å. The Born-von Karman boundary condition is applied for each primitive unit cell obtained with multiplication after steps (3) and (4) for the phonon calculation. In these calculations, the primitive cells are multiplied by 2 for each direction of the unit vector.

III. RESULTS AND DISCUSSIONS

The structure with K_4 crystal frame considered for C, XC_2 , Si and $SrSi_2$ systems in the present study maintain K_4 type crystal frame composed of C or Si with distortion through the whole process of the geometry optimization. Furthermore, the crystal symmetry is maintained with an accuracy of less than 0.001 Å. The lattice constant (a), volume at lattice constant (V_0), cohesive energy per atom (E_{coh}) and bulk modulus at V_0 (B_0) are evaluated for the fully optimized structure. In this study, E_{coh} for XC_2 : $E_{\text{coh};XC_2}$ is defined as

$$E_{\text{coh};XC_2} = \frac{E_{XC_2} + N_X \text{ atom } E_{X \text{ atom}} + N_C \text{ atom } = K_4 E_{C \text{ atom}}}{N_X \text{ atom} + N_C \text{ atom} = K_4} ;$$

Here, E_A and N_A are the total energy and the number of atoms for A, respectively. To obtain these values, Muraghan's equation of state is used to fit the binding energy versus volume curve. Parameters in the equation are determined using the least squares method in the range of about $0.8V_0 < V < 1.2V_0$, where the root mean square is set to be less than 5.0 meV/atom.

The obtained values of a , V_0 , E_{coh} , and B_0 for the crystals are shown in Figure 2 (a). In XC_2 , the values of a and V_0 generally increase with the atomic number of X. Generally, the values of a for the XC_2 crystals are larger than that for carbon K_4 . That is, generally the carbon K_4 frames are expanded by intercalating X to the carbon systems.

However, the values of V_0 for X = H, Li, ..., S, are smaller than that of carbon K_4 while those for X = Cl, ..., Sr are larger. This is because of the sufficiently wide

vacant spaces in carbon K_4 that is compensated by X atoms and the increase of the occupied spaces by X atoms for the increase of the atomic number of X.

On the other hand, the values of E_{coh} decrease with the increasing period of X. There is a strong negative correlation with a and V_0 as shown in the correlation coefficients: $r_{a E_{\text{coh}}} = -0.792$ and $r_{V_0 E_{\text{coh}}} = -0.796$. For each period of X in the XC_2 , E_{coh} generally shows largest values for intermediate elements X: III B or IV B. This enhanced energy gain can be explained by the completion of the electronic shell in C atoms composing K_4 type frame, the bonds formation with X in the XC_2 crystals and the bonds expansion which weaken the bonds. The E_{coh} values of the XC_2 are not larger than that of the carbon K_4 . This is apparently resulted from the relative weakness of the X-C bonds in the XC_2 crystals compared with the C-C bonds in the carbon K_4 crystal. Subsequently, the absence of correlation between E_{coh} and dynamical stability is shown.

The values of B_0 also decrease with the increasing period of X, similar to the case of E_{coh} . The B_0 s of XC_2 are generally smaller than that of C. There is a strong correlation between B_0 and E_{coh} as indicated by the correlation coefficient: $r_{E_{\text{coh}} B_0} = 0.848$.

From the values of a and V_0 in Si and $SrSi_2$, the relation shown in the C and XC_2 systems also seems to hold for the Si and XS_2 systems. However, the values of E_{coh} and B_0 of $SrSi_2$ are larger than those of Si. This relation is apparently different from the cases of C and XC_2 systems. This can be attributed to the X-Si bond strength being much higher than that of the Si-Si bonds in XS_2 .

To understand the correlation between the stability and the structure in detail, the nearest-neighbour distances between different atoms specified in Fig. 1 (e) d_{C-C} , d_{X-C_A} , d_{X-C_B} , d_{X-C_C} , \bar{d}_{X-C} (the average of all d_{X-C}) and d_{X-X} as well as the angle $\angle X-C_A-C_B$, and the minimal dihedral angle for the nearest-neighbour C atoms $\angle C-C-C-C$ are investigated.

As shown in Fig. 2 (b), in general d_{C-C} , \bar{d}_{X-C} and d_{X-X} increase with the increasing atomic number in X, similar to the cases of a and V_0 . The d_{C-C} and \bar{d}_{X-C} show very strong correlation with the a , indicated by the correlation coefficients: $r_{a d_{C-C}} = 0.930$ and $r_{a \bar{d}_{X-C}} = 0.987$. These distances have also correlation with E_{coh} : $r_{E_{\text{coh}} d_{C-C}} = -0.630$ and $r_{E_{\text{coh}} \bar{d}_{X-C}} = -0.741$, although the values are smaller.

It is apparent that the correlations shown in \bar{d}_{X-C} with a and E_{coh} are resulted from the very strong correlation of d_{X-C_A} and d_{X-C_B} with a and E_{coh} as indicated by the correlation coefficients: $r_{a d_{X-C_A}} = 0.824$, $r_{a d_{X-C_B}} = 0.973$, $r_{a d_{X-C_C}} = 0.180$, $r_{E_{\text{coh}} d_{X-C_A}} = -0.759$, $r_{E_{\text{coh}} d_{X-C_B}} = -0.796$, and $r_{E_{\text{coh}} d_{X-C_C}} = -0.051$.

Here, it should be noted that the each inequivalent atomic distance between X and C: d_{X-C_A} , d_{X-C_B} , and d_{X-C_C} show interesting X dependence. The XC_2 systems with X of 3rd, 4(5)th periods show distinct differences between X = IA and IIA, and other Xs. In the compound

with $X = \text{IA}$ or IIA , the $dX-C_A$ and $dX-C_B$ are relatively larger while $dX-C_C$ is smaller compared with those of the other compounds with X of the neighbour atomic number. The angle $\angle X-C_A-C_B$ show distinct smaller values for the compounds with $X = \text{IA}$ and IIA and this is attributed to the X dependence of the $dX-C_A$ and $dX-C_B$. The dihedral angle $\angle C-C-C-C$ shown in Tab. II also show smaller values for the compounds with $X = \text{IA}$ or IIA although the differences with other compounds are very small. Apparently, those differences are due to the number of the outer most valence electrons in X . However, an exceptional trend is shown in the systems with X of 2nd period for those values and the trend can be attributed to the elemental closeness between the X and C .

The relative position of X in the crystal is maintained resulting in $r_{\text{ad}_X} = 1.000$. Therefore, $dX-X$ can be considered as a standard distance in the XC_2 systems. To emphasize the similarity of the structures, various distance ratios of the nearest-neighbour distances to $dX-X$ are shown in Fig. 2(c). Although significant larger (smaller) $dC-C / dX-X$, $dX-C / dX-X$, and $dC-C_C / dX-X$ ($dC-C_A / dX-X$) are shown in the crystals with $X = C, N$, and O , these ratios are almost constant in the same group of X .

In Figure 3, the phonon density of states (DOS) without step (4) for C and XC_2 ($X = H, Li, Be, B, C, N, O, F, Na, Mg, Al, Si, P, S, Cl, K, Ca, Ga, Ge, As, Se, Br, Rb$ or Sr), Si and $SrSi_2$ with K_4 type am e of C or Si are depicted. From the above discussions and Fig. 2(a), the intermediate value of a realized for the compounds with X in 3rd (4th) (4.5-4.8 Å) and the accompanied interatomic distances in these crystals seem to make the band narrower. Namely, the interatomic distances roughly determine the vibrational frequency range in these crystals. The imaginary frequency modes rarely appear in NaC_2 , MgC_2 and $SrSi_2$ although they appear in relatively wide imaginary frequency range in C and Si .

For the structures of C , NaC_2 , MgC_2 , Si and $SrSi_2$ obtained after step (4), the phonon DOS and dispersion relationship are also evaluated. As shown in Fig. 4, the phonon DOS for the fully optimized structures of the other XC_2 crystals show almost the same shapes as those of the optimized structures from step (3). Therefore, it is expected that the discussion in the previous paragraph is significant and skipping step (4) is expected to be effective for reducing the computational cost in this study.

As shown in Figure 4, in carbon K_4 , although the imaginary frequency mode is not appear at the Γ point, it appear in wide range of other k points as indicated by Yao et al⁵. On the other hand, silicon K_4 has imaginary modes even at the Γ point. Namely, the carbon and silicon K_4 crystal structures are on a high rank of saddle points in those potential energy surfaces and the lifetimes of them are expected to be very short in nature.

On the other hand, in our calculations although NaC_2 , MgC_2 and $SrSi_2$ have imaginary frequencies in the acoustic modes slightly around the Γ point, there are no imagi-

nary modes in the other k points. These suggest that those structures are stable although they break the structures against the phonon vibration with long wave length limit. The existence of the $SrSi_2 K_4$ in nature⁶ suggests that the results in this study based on the density functional theory can predict the thermal stability of the structure. From this fact and the calculation results, the stable existence of K_4 type crystal structures in NaC_2 and MgC_2 is expected in nature although they do not realize maximum E_{coh} in the considered XC_2 crystals.

From the maximum frequencies obtained for diamond (1300 cm^{-1} for C^{18} , 500 cm^{-1} for Si^{19}) and graphite (1600 cm^{-1} for C^{18}), the orders of both $C-C$ and $Si-Si$ chemical bonds can be considered less than 1, as discussed by Yao et al⁵. Therefore, based on the rough expectation from the monoatomic systems, the orders are expected to be less than 1 between the atoms composing K_4 type am e of NaC_2 , MgC_2 and $SrSi_2$ crystals. The characters of chemical bonds are analysed from the valence charge distribution as described below.

To understand the stability of the K_4 systems, the valence charge distributions are analysed. Fig. 5 shows various types of distribution in the conventional or the primitive unit cells for the fully optimized C , NaC_2 , MgC_2 , Si and $SrSi_2$ crystals with K_4 type am e. Fig. 5(a) details planes selected to show the distribution of quantities noted in Figs. 5(c), (e), and (g). The populations around the Sr atoms are neglected for easier comparison in Figs. 5(c) and (e).

Figures 5(b) and (c) show the isosurface and contour of charge density. Apparently, the valence charge is locally distributed along the lines between adjacent C or Si atoms of the K_4 type am e for the considered systems. It should be noted that a distinctive difference appears between the charge distribution of the C (XC_2) and Si ($SrSi_2$) crystals in the intermediate region between the nearest-neighbour atoms in those am es. The charge is more localized to the C than Si atoms. These features are also indicated in the diamond crystal structures as shown in the previous studies²⁰. It can be said that the atomic intercalation change the distribution slightly. However, as discussed for the phonon frequencies, this quantity is sufficient to change the properties of the crystals.

Figures 5(d) and (e) show the differences between the valence charge density of the crystals (ex. $n_{NaC_2}(r)$) and their separated components: the intercalated atoms (ex. $n_{Na}(r)$) and the am e (ex. $n_{C_2}(r)$). As shown in Fig. 5(d), the significant excess charge is shown in the region between the adjacent $Na-C$, $Mg-C$ and $Sr-Si$ for NaC_2 , MgC_2 and $SrSi_2$, respectively; therefore suggesting bond creation in those regions. Furthermore, as shown in Fig. 5(e), in NaC_2 , MgC_2 and $SrSi_2$, the charge accumulations increase in the region of σ type orbitals while those decrease along the π type bonds; suggesting that the π type bonds are strengthened and the σ type bonds are weakened. On the other hand, the maximum frequency of the phonon modes shown in Fig. 4 is less than the monoatomic systems. Therefore, the net bond orders in

the K_4 type am e are expected to be decreased by the atomic intercalation.

Here, the nature of the bonds is noted from the information of the ELF. Figs. 5(f) and (g) show the isosurface (0.8 \AA^{-3}) and the contour. As shown here, C, NaC_2 , MgC_2 , Si and SrSi_2 has similar ELF distribution between the adjacent C-C and Si-Si. However, the feature of type bonds formation is strengthened with significance. The relatively smaller value of $\langle C-C-C-C \rangle$ ($\langle Si-Si-Si-Si \rangle$) seems to have correlation with this feature. The strengthened type bonds seem to stabilize the structures against the thermal vibration. From the comparison with the case of graphite, the absence of the type bonds indicated by Yao et al.⁵, is not confirmed in our calculations.

The stabilization of atomic intercalated carbon crystals is realized from delicate balance of bonding. As shown in the valence charge density, the formation of strongly polarized type bonds between Na or Mg and C_A and the strength enhanced bonds seems to stabilize the structure of NaC_2 and MgC_2 . The discriminative stability seems to be realized by the properous atomic radii of X and the completion or near completion of the electronic shell of the each C atom in the K_4 type am e by $X = \text{IA}$ or IIA . Similar mechanism of the stability is expected to exist in the Si and XSi_2 systems.

Figure 6 shows X-ray diffraction (XRD) patterns of the fully optimized crystal structure of C, NaC_2 , MgC_2 , Si and SrSi_2 . Monochromatic radiation with wave length 1.541 \AA is assumed in these calculations. As shown in this figure, the compounds have specific XRD peaks at larger 2θ compared with the pure K_4 crystals.

Figure 7 shows the electron band structures, DOS, and local DOS of valence electrons for the atoms composing K_4 type am e and the intercalated atoms in the fully optimized C, NaC_2 and MgC_2 and the Si and SrSi_2 crystals, respectively. From the bottom energy levels to the upper levels, the angular momentum for the electronic states successively changes in the order of s, p and d character, although every component appears in most states. From the bottom energy levels to those around the Fermi level, the band structures are similar in these crystals. NaC_2 and MgC_2 K_4 show a metallic and semiconducting feature, respectively, while carbon K_4 is metallic. As shown in Fig. 6, both Si and SrSi_2 have metallic features. It is noteworthy that the previous first principles calculations for SrSi_2 ¹⁷ also show qualitatively the same result with the present calculation.

IV. CONCLUSIONS AND SUMMARY

The stability of the atomic intercalated carbon K_4 crystals, XC_2 ($X = \text{H, Li, Be, B, C, N, O, F, Na, Mg, Al, Si, P, S, Cl, K, Ca, Ga, Ge, As, Se, Br, Rb, and Sr}$), are evaluated from the geometry optimization and the frozen phonon analysis based on the first principles calculations. NaC_2 and MgC_2 are found to be stable although C K_4 is not stable. The formation of strongly

polarized type bonds between Na or Mg and C_A and the strength enhanced bonds seems to stabilize the structure of NaC_2 and MgC_2 . The discriminative stability seems to be realized by the properous atomic radii of X and the completion or near completion of the electronic shell of the each C atom in the K_4 type am e by $X = \text{IA}$ or IIA . The NaC_2 and MgC_2 are found to be metallic and semiconducting, respectively.

V. APPENDIX

The values presented in Figure 2 are listed in Table I and II.

Acknowledgements

The authors acknowledge staff of the CCM S, IM R for allowing the use of the HITACHI SR11000 supercomputing facilities. The authors acknowledge Professor Motoko Kotani and Professor Toshikazu Sunada for information about the crystal structure of SrSi_2 . We also acknowledge financial support from the CREST, MEXT, and WPI.

-
- ¹ T. Sunada, *Not. Amer. Math. Soc.*, **55**, 208 (2008).
 - ² Y. Kawazoe, T. Kondow, and K. Ohno, Eds., *Clusters and Nanomaterials*, Springer (2002), and references therein.
 - ³ G. M. Rignanes and J.-C. Charlier, *Phys. Rev. B*, **78**, 125415 (2008).
 - ⁴ M. Itoh, M. Kotani, H. Naito, T. Sunada, Y. Kawazoe, and T. Adachi, *Phys. Rev. Lett.*, **102**, 055703 (2009).
 - ⁵ Y. Yao, J. S. Tsai, J. Sun, D. D. Klug, R. Martonak, and T. Itaka, *Phys. Rev. Lett.*, **102**, 229601 (2009).
 - ⁶ K. Janson, H. Schafer, and A. Weiss, *Angew. Chem. Int. Ed.*, **4**, 245 (1965).
 - ⁷ U. Ruschewitz, *Coord. Chem. Rev.*, **244**, 115 (2003).
 - ⁸ P. Hohenberg, and W. Kohn, *Phys. Rev.*, **136**, B 864 (1964).
 - ⁹ W. Kohn, and L. J. Sham, *Phys. Rev.*, **140**, A 1133 (1965).
 - ¹⁰ G. Kresse, and J. Furthmüller, *Phys. Rev. B*, **54**, 11169 (1996).
 - ¹¹ J. P. Perdew, and A. Zunger, *Phys. Rev. B*, **23**, 5048 (1981).
 - ¹² D. M. Ceperley, and B. J. Alder, *Phys. Rev. Lett.*, **45**, 566 (1980).
 - ¹³ P. E. Blochl, *Phys. Rev. B*, **50**, 17953 (1994).
 - ¹⁴ F. D. M. Umagahan, *Proc. Natl. Acad. Sci. USA*, **30**, 244 (1944).
 - ¹⁵ A. Togo, FROPHO, <http://frophi.sourceforge.net/>
 - ¹⁶ K. Parlinski, Z. Q. Li, and Y. Kawazoe, *Phys. Rev. Lett.*, **78**, 4063 (1997).
 - ¹⁷ Y. Imai, and A. Watanabe, *Intermetallics*, **10**, 333 (2002).
 - ¹⁸ T. Tohei, A. Kuwabara, F. Oba, and I. Tanaka, *Phys. Rev. B*, **73**, 064304 (2006).
 - ¹⁹ P. Giannozzi, S. Giannozzi, P. Pavone, and S. Baroni, *Phys. Rev. B*, **43**, 7231 (1991).
 - ²⁰ M. L. Cohen, *Science*, **234**, 4776 (1986).
 - ²¹ A. Kokalj, *Comp. Mat. Sci.*, **28**, 155 (2003).

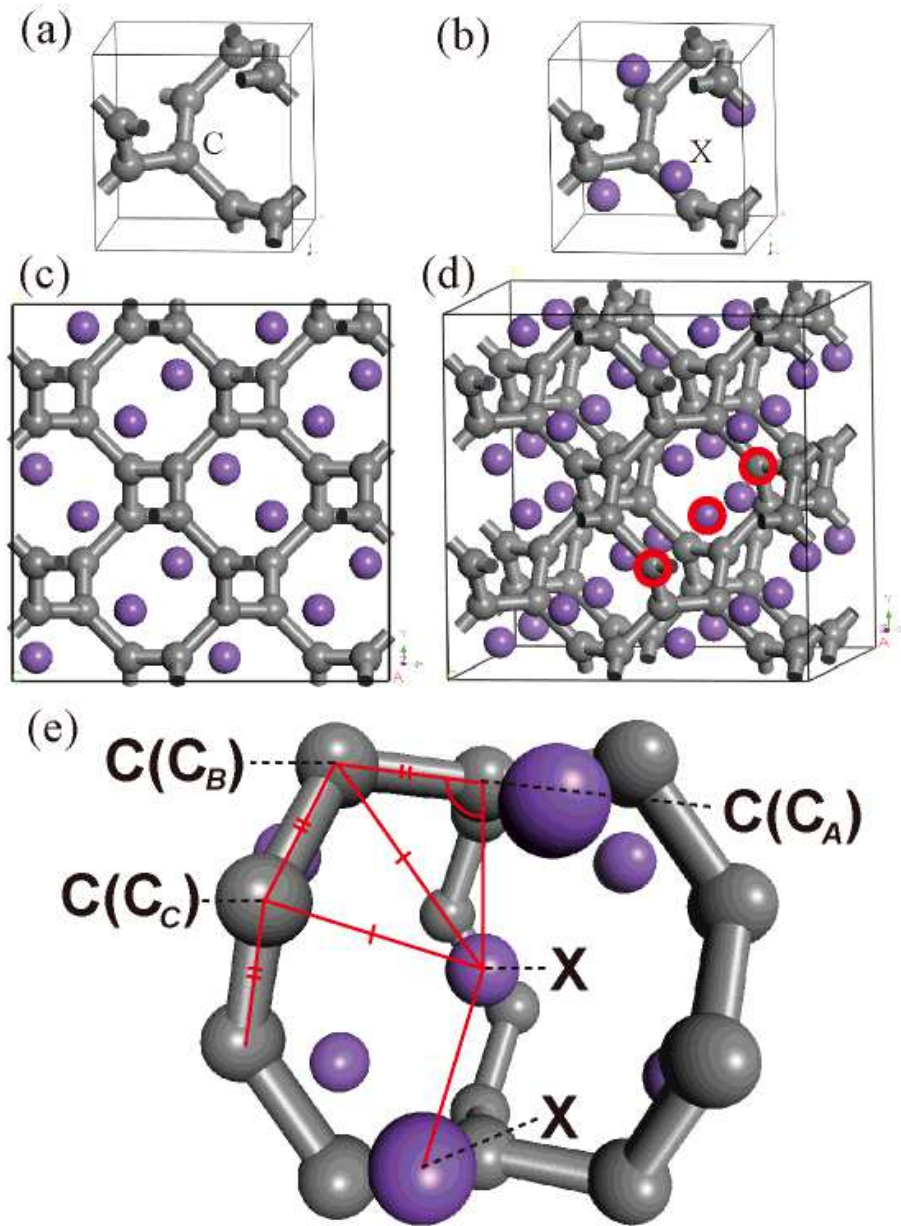


FIG. 1: (a) The conventional unit cell of the carbon K₄ crystal with I₄132(O₈) symmetry. (b) Initial structure of the primitive unit cell of XC₂ crystal with K₄ space group of C with P₄332(O₆) symmetry. (c) 2 × 2 × 2 super cell of the (b). The symmetric plane of the impurity intercalated system. (d) Three adjacent atoms (C-X-C) that align in a straight line with equivalent distance (C-X and X-C) are encircled with red thick line in (c). (e) An extracted structure. The C atoms can be classified into C_A, C_B and C_C.

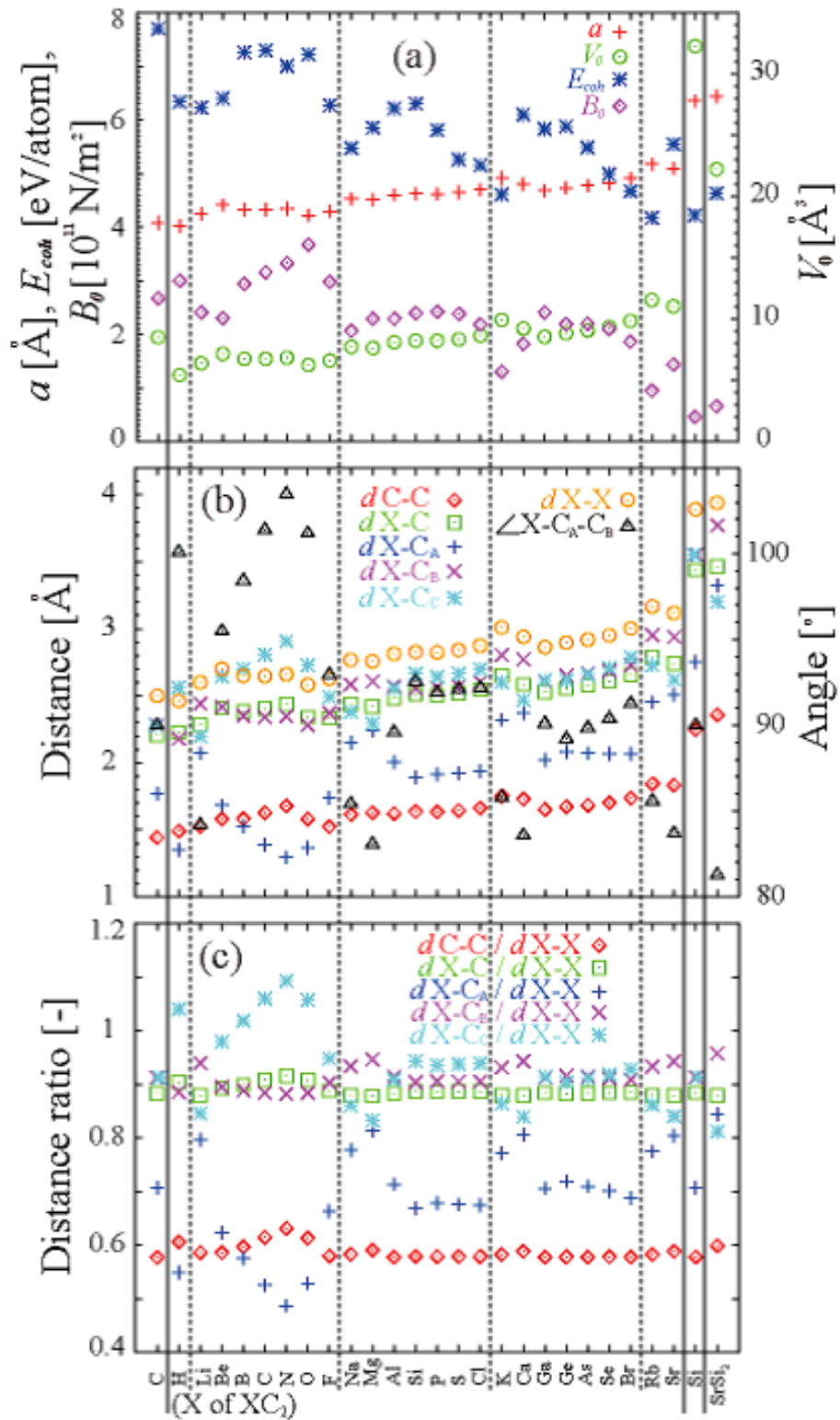


FIG. 2: (a) Determined lattice constant (a), volume at a (V_0), cohesive energy (E_{coh}), and bulk modulus at V_0 (B_0), and (b) the nearest-neighbour distances and angles for the fully optimized C , XC_2 , Si , and $SrSi_2$ crystal structures with K_4 type anion within LDA. The classification of the C (Si) atoms (C_A , C_B , and C_C) is based on the irreducibility of the crystal symmetry as shown in Fig. 1. (c) The distance ratios.

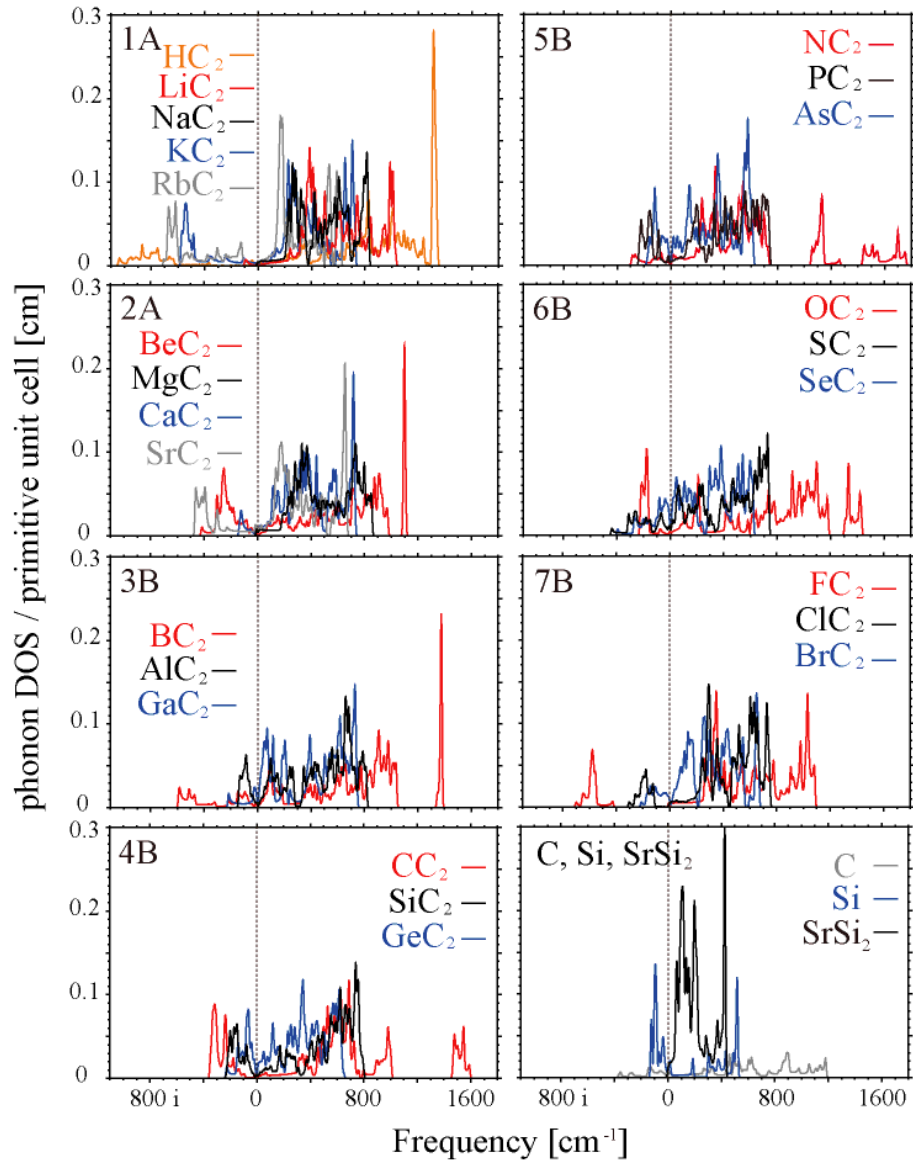


FIG. 3: Phonon density of states (DOS) of XC_2 ($X = H, Li, Be, B, C, N, O, F, Na, Mg, Al, Si, P, S, Cl, K, Ca, Ga, Ge, As, Se, Br, Rb$ and Sr), C, Si and $SrSi_2$ crystal with K_4 type anion of C , or Si . The structures are obtained from geometry optimization under symmetry constraint to the initial structures.

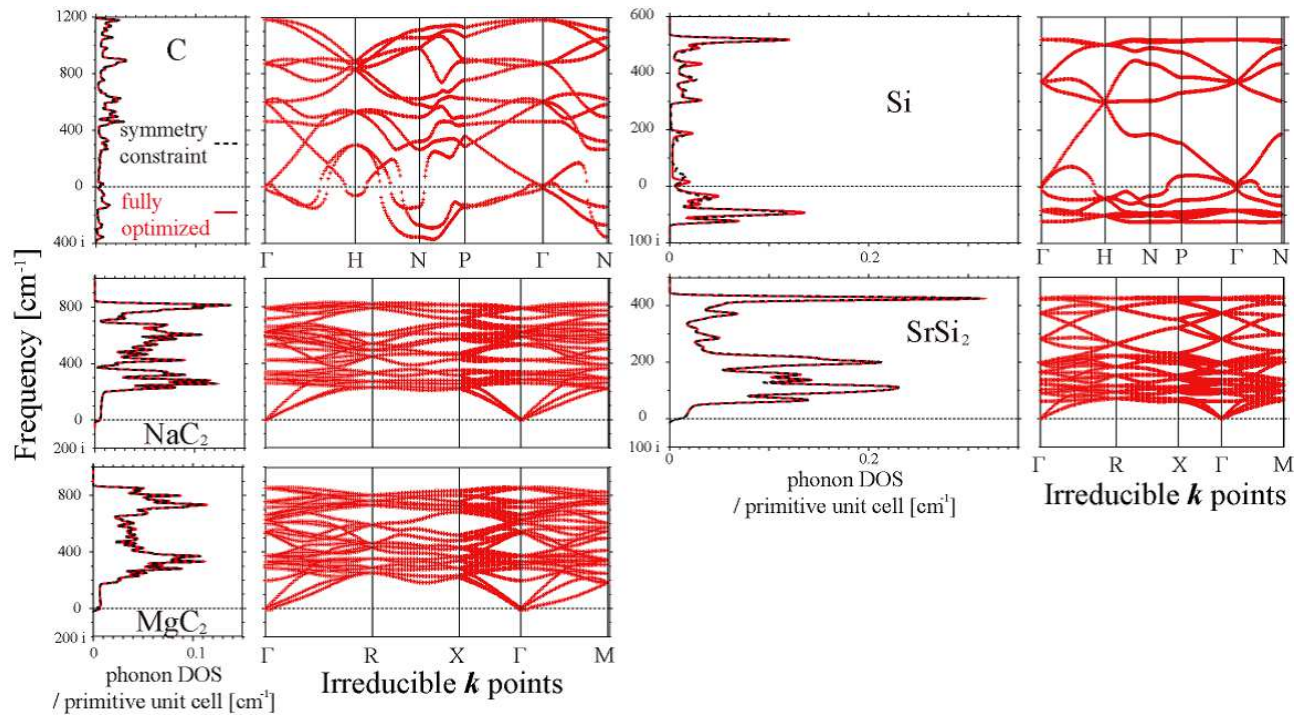


FIG. 4: (Left) Phonon density of states (DOS) of partially and fully optimized structures of C, NaC₂, MgC₂, Si and SrSi₂ with K₄ type anion of C or Si. (Right) The phonon dispersion relationship for the fully optimized structures.

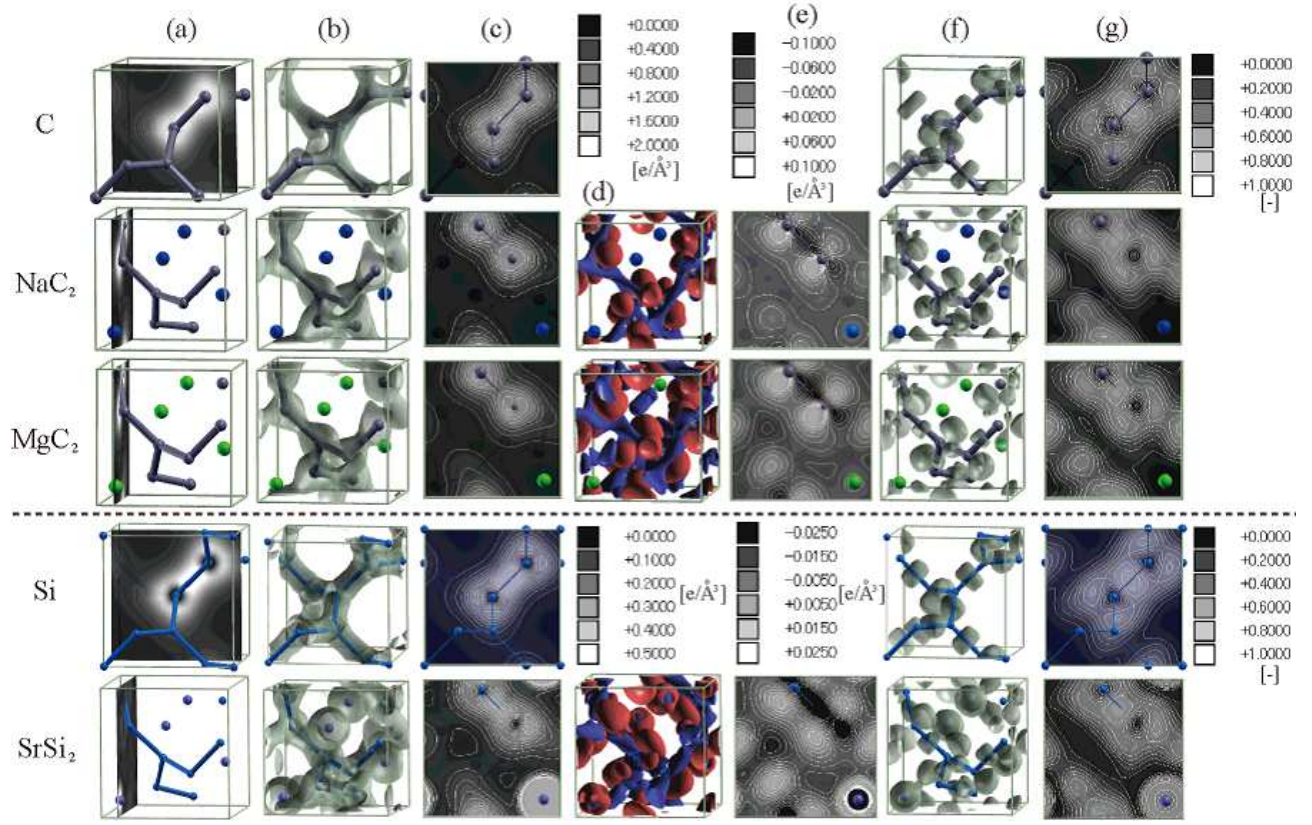


FIG. 5: (a) The conventional or the primitive unit cells for the fully optimized C, NaC₂, MgC₂, Si and SrSi₂ crystals with K₄ type of anion of C or Si. The planes are selected to show the distribution of the valence charge density, difference between the valence charge density of the crystals (ex. $\rho_{\text{NaC}_2}(\mathbf{r})$) and their separated components: the intercalated atoms (ex. $\rho_{\text{Na}}(\mathbf{r})$) and the anion (ex. $\rho_{\text{C}_2}(\mathbf{r})$), and the electronic localization function (ELF). The isosurfaces of the valence charge density (1.5, 1.0, 1.0, 0.35 and 0.35 e/Å³ for C, NaC₂, MgC₂, Si and SrSi₂, respectively) (b) and the contours (c). The isosurfaces of the differences of the valence charge density (0.05, 0.05 and 0.025 + (-) e/Å³ coloured with red (blue) for NaC₂ and SrSi₂, respectively) (d) and the contours (e). The isosurfaces of the ELF (0.8 [-]) (f) and the contours (g). For (c) and (e), the high population around the Sr atoms is neglected for easier comparison. XCrySDen²¹ was used for the visualization.

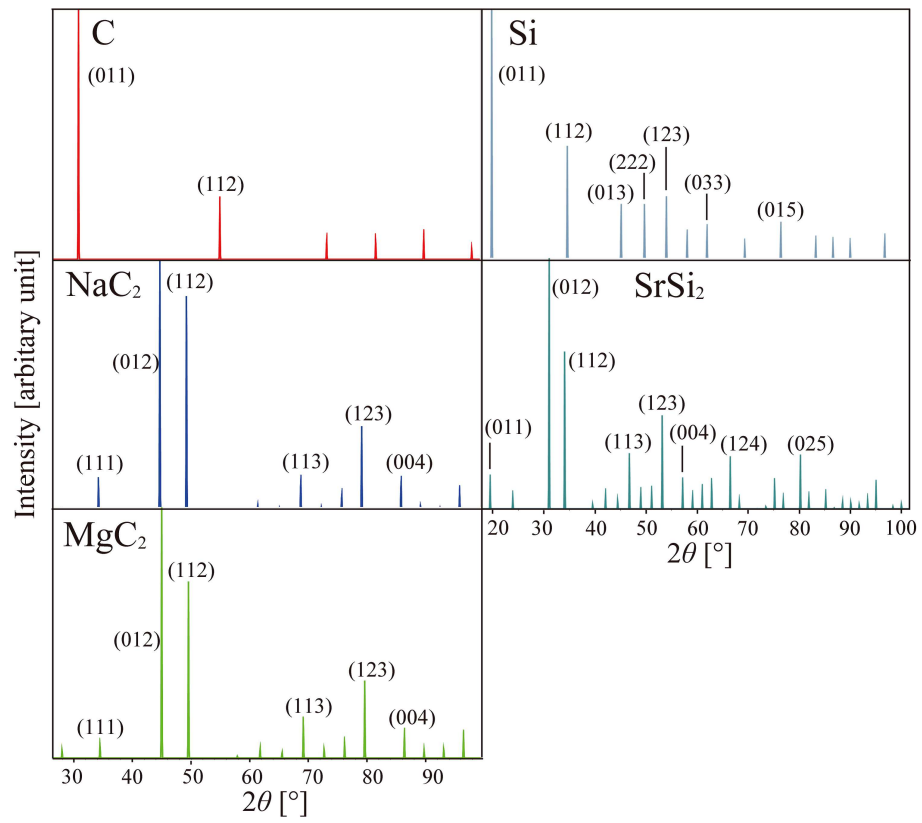


FIG. 6: XRD patterns for the fully optimized structures of C, NaC₂, MgC₂, Si and SrSi₂ with K₄ type structure of C or Si.

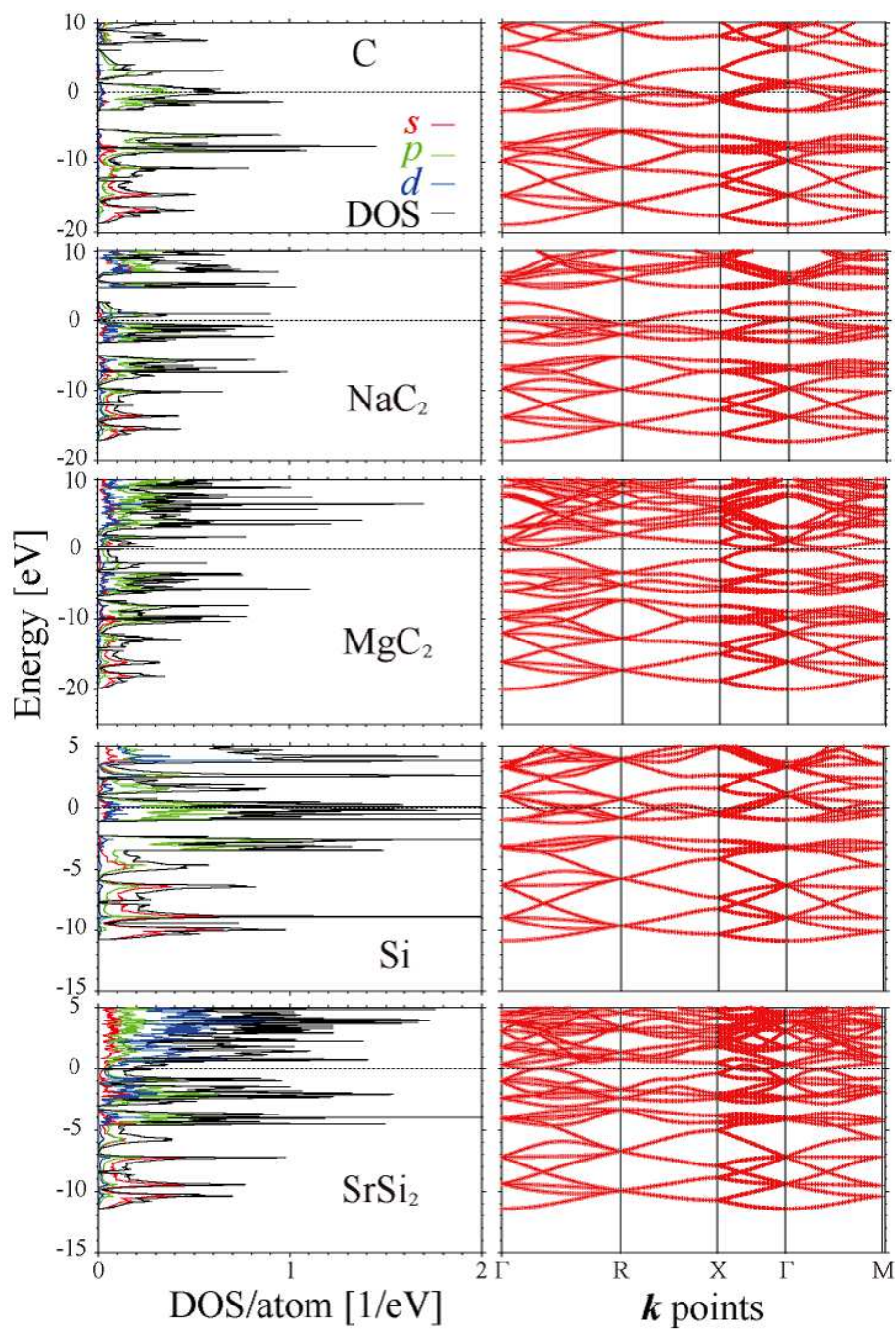


FIG. 7: Electronic density of states (DOS) and the dispersion relationship for the fully optimized conventional or primitive unit cells of C, NaC₂, MgC₂, Si and SrSi₂ crystals with K₄ type frame of C or Si.

TABLE I: Determined lattice constant (a), volume at a (V_0), cohesive energy (E_{coh}), and bulk modulus at V_0 (B_0) for the fully optimized C , XC_2 , Si and $SrSi_2$ crystal structures with K_4 type anion within LDA.

Component	a [Å]	V_0 [Å ³ /atom]	E_{coh} [eV/atom]	B_0 [$10^{11} \frac{N}{m^2}$]
C^4	4.082	8.502	7.702	2.67
HC_2	4.025	5.433	6.335	3.00
LiC_2	4.250	6.396	6.231	2.41
BeC_2	4.412	7.158	6.401	2.30
BC_2	4.328	6.758	7.259	2.94
CC_2	4.326	6.747	7.295	3.16
NC_2	4.348	6.850	7.003	3.33
OC_2	4.218	6.252	7.221	3.67
FC_2	4.296	6.607	6.273	2.98
NaC_2	4.526	7.728	5.476	2.06
MgC_2	4.506	7.623	5.856	2.29
AlC_2	4.598	8.102	6.214	2.29
SiC_2	4.622	8.227	6.301	2.39
PC_2	4.619	8.214	5.805	2.42
SC_2	4.644	8.345	5.261	2.38
ClC_2	4.699	8.646	5.152	2.18
KC_2	4.920	9.926	4.606	1.30
CaC_2	4.803	9.232	6.099	1.82
GaC_2	4.679	8.536	5.831	2.41
GeC_2	4.731	8.823	5.875	2.19
AsC_2	4.773	9.059	5.485	2.20
SeC_2	4.823	9.351	4.987	2.10
BrC_2	4.908	9.852	4.668	1.86
RbC_2	5.175	11.550	4.172	0.95
SrC_2	5.096	11.030	5.545	1.44
Si	6.354	32.089	4.220	0.46
$SrSi_2$	6.436	22.216	4.634	0.66

TABLE II: Determined nearest-neighbour distances and angles for the fully optimized C , XC_2 , Si and $SrSi_2$ crystal structures with K_4 type anion within LDA. The classification of the C (Si) atoms (C_A , C_B and C_C) is based on the irreducibility of the crystal symmetry as shown in Fig. 1. The smallest dihedral angles for the nearest-neighbor C (Si) atoms of K_4 anion are also shown.

Component	d_{C-C} [Å]	\overline{d}_{X-C} [Å]	d_{X-C_A} [Å]	d_{X-C_B} [Å]	d_{X-C_C} [Å]	d_{X-X} [Å]	$\angle X-C_A-C_B$ [°]	$\angle C-C-C$ [°]
C^4	1.443	2.209	1.768	2.282	2.282	2.500	90.000	70.529
HC_2	1.492	2.226	1.350	2.180	2.563	2.463	100.081	67.946
LiC_2	1.525	2.286	2.071	2.444	2.199	2.601	84.183	69.686
BeC_2	1.581	2.409	1.683	2.417	2.644	2.701	95.477	69.782
BC_2	1.582	2.383	1.526	2.354	2.698	2.650	98.434	68.732
CC_2	1.628	2.405	1.391	2.341	2.808	2.649	101.393	67.330
NC_2	1.679	2.437	1.295	2.347	2.908	2.661	103.471	67.202
OC_2	1.582	2.343	1.365	2.282	2.729	2.582	101.180	65.807
FC_2	1.524	2.333	1.741	2.372	2.492	2.628	92.955	70.313
NaC_2	1.614	2.436	2.152	2.585	2.381	2.769	85.408	70.005
MgC_2	1.628	2.422	2.244	2.608	2.295	2.757	83.057	69.323
AlC_2	1.624	2.483	2.006	2.572	2.554	2.813	89.592	70.525
SiC_2	1.637	2.508	1.890	2.555	2.666	2.827	92.542	70.369
PC_2	1.634	2.503	1.916	2.559	2.643	2.825	91.904	70.439
SC_2	1.645	2.520	1.920	2.573	2.666	2.843	92.100	70.420
CCl_2	1.663	2.548	1.938	2.601	2.698	2.874	92.170	70.412
KC_2	1.752	2.649	2.322	2.804	2.602	3.011	85.787	70.088
CaC_2	1.730	2.584	2.369	2.773	2.466	2.940	83.574	69.498
GaC_2	1.653	2.530	2.020	2.613	2.617	2.863	90.101	70.529
GeC_2	1.673	2.556	2.082	2.653	2.617	2.896	89.211	70.513
AsC_2	1.685	2.578	2.071	2.667	2.659	2.919	89.841	70.528
SeC_2	1.704	2.608	2.069	2.689	2.707	2.951	90.387	70.525
BrC_2	1.736	2.659	2.067	2.728	2.787	3.004	91.257	70.490
RbC_2	1.845	2.786	2.453	2.954	2.729	3.167	85.575	70.042
SrC_2	1.834	2.740	2.507	2.939	2.619	3.118	83.684	69.533
Component	d_{Si-Si} [Å]	d_{X-Si} [Å]	d_{X-Si_a} [Å]	d_{X-Si_b} [Å]	d_{X-Si_c} [Å]	d_{X-X} [Å]	$\angle X-Si_a-Si_b$ [°]	$\angle Si-Si-Si$ [°]
Si	2.247	3.439	2.752	3.553	3.553	3.891	90.000	70.529
$SrSi_2$	3.463	2.358	3.324	3.772	3.200	3.941	81.270	68.605